12-1-2014

Crossover in the magnetic response of single-crystalline Ba1−xKxFe2As2 and Lifshitz critical point evidenced by Hall effect measurements

Yong Liu
Iowa State University, yliu@ameslab.gov

Thomas A. Lograsso
Iowa State University, lograsso@ameslab.gov

Crossover in the magnetic response of single-crystalline $Ba_{1-x}K_xFe_2As_2$ and Lifshitz critical point evidenced by Hall effect measurements

Yong Liu[1,*] and Thomas A. Lograsso[1,2]

[1]*Division of Materials Sciences and Engineering, Ames Laboratory, Ames, Iowa 50011, USA*

[2]*Department of Materials Science and Engineering, Iowa State University, Ames, Iowa 50011, USA*

(Received 10 June 2014; revised manuscript received 11 November 2014; published 5 December 2014)

We report on the doping evolution of magnetic susceptibility $\chi(T)$ and Hall coefficient R_H in high-quality $Ba_{1-x}K_xFe_2As_2$ ($0.13 \leqslant x \leqslant 1$) single crystals. It is found that the normal-state magnetic susceptibility of $Ba_{1-x}K_xFe_2As_2$ compounds undergoes a crossover from linear-T dependence in the undoped and underdoped samples into KFe_2As_2-type magnetic response in the overdoped samples with increasing K content. Although magnetic susceptibility $\chi(T)$ of optimally doped samples ($0.34 \leqslant x \leqslant 0.47$) still follows a monotonic increase with increasing temperature, a big hump around 300 K emerges. As x exceeds 0.53, a broad peak forms in overdoped samples ($0.53 \leqslant x \leqslant 1$), which shifts toward 120 K for the end member KFe_2As_2. Above the peak temperature $T^* = 120$ K, a Curie-Weiss-like behavior is observed in KFe_2As_2. The Hall coefficient R_H of underdoped sample $x = 0.22$ shows a rapid increase above spin-density-wave transition temperature T_{SDW}. Below T_{SDW}, it increases slowly. R_H of optimally doped and slightly overdoped samples ($0.34 \leqslant x \leqslant 0.65$) shows relatively weak temperature dependence and a saturation tendency below 150 K. However, R_H of K heavily overdoped samples ($0.80 \leqslant x \leqslant 1$) increases rapidly below 150 K. Meanwhile, the Hall angle $\cot\theta_H$ displays a concave temperature dependence within the doping range $0.22 \leqslant x \leqslant 0.55$, whereas it changes to a convex temperature dependence within the doping range $0.65 \leqslant x \leqslant 1$. The dramatic change coincides with the Lifshitz transition occurring around the critical doping $x = 0.80$, where angle photoemission spectroscopy measurements had confirmed that the electron pocket disappears with excess hole doping in the $Ba_{1-x}K_xFe_2As_2$ system. It is suggested that the characteristic temperature T^* at around $120 \sim 150$ K observed in susceptibility and the Hall coefficient, as well as previously reported resistivity data, may indicate an incoherence-coherence crossover in the $Ba_{1-x}K_xFe_2As_2$ system.

DOI: 10.1103/PhysRevB.90.224508 PACS number(s): 74.70.Xa, 74.25.F−, 75.30.Cr

I. INTRODUCTION

Novel magnetism and multiband structure are two key aspects in the research of iron-based superconductors [1–6]. Parent compounds such as LaOFeAs and $BaFe_2As_2$ show a spin-density-wave (SDW) transition at T_{SDW} 140 K [7,8], coupled with a phase transition from tetragonal to orthorhombic structures. The normal state of iron-based superconductors is a strongly correlated metal and the parent compound is a bad metal at the verge of the metal-insulator transition [9]. By aliovalent and isovalent ion doping or an application of pressure, the SDW order is suppressed, while a superconducting dome emerges with increasing doping levels in the phase diagram [1,2]. The primary pairing interaction was proposed to be mediated by antiferromagnetic (AFM) spin fluctuations. As a result, the superconducting state was expected to be the $s_\pm$ state, i.e., extended s-wave pairing with a sign reversal of the order parameter between different Fermi surface sheets [10]. Among the iron-based superconductors, the $Ba_{1-x}K_xFe_2As_2$ system is quite unique. The optimally doped sample $x = 0.4$ displays a T_c of 38 K. With increasing K doping level, T_c steadily decreases to 3.8 K for the end member KFe_2As_2 [11]. It was found that the electronic structure of $Ba_{1-x}K_xFe_2As_2$ compounds shows a dramatic change from optimally doped to overdoped samples [12,13]. Accompanied with the evolution of electronic structure, the pairing symmetry seems to change from $s_\pm$ wave in optimally doped samples to d wave in KFe_2As_2 [14]. Recent angle-resolved photoemission spectroscopy (ARPES) found that the Fermi surface (FS) topology of the $Ba_{0.1}K_{0.9}Fe_2As_2$ single crystal is similar to that of KFe_2As_2, but differs from that of $Ba_{0.3}K_{0.7}Fe_2As_2$, which was interpreted within the framework of the Lifshitz transition occurring between $0.7 < x < 0.9$ [15]. Theoretical calculations also pointed out that the dissolution of electron cylinders occurs near $x \sim 0.9$ with Lifshitz transition in $Ba_{1-x}K_xFe_2As_2$ superconductors [16]. The doping-dependent FS reconstruction is also evidenced by the change of thermoelectric power S_{ab} for overdoped $Ba_{1-x}K_xFe_2As_2$ single crystals, where the maximum at around 120 K in temperature dependence of S_{ab} collapses into a plateau at $x \sim 0.8$–0.9 [17].

The transport property of the $Ba_{1-x}K_xFe_2As_2$ system also shows different behavior, compared to electron-doped $Ba(Fe_{1-x}Co_x)_2As_2$ and isovalent-doped $BaFe_2(As_{1-x}P_x)_2$. A linear-T dependence of in-plane resistivity ρ_{ab} was universally observed in the optimally doped $BaFe_2(As_{1-x}P_x)_2$ [18], $Ba(Fe_{1-x}Co_x)_2As_2$ [19], and $Ba(Fe_{1-x}Ni_x)_2As_2$ [20] single crystals, while the Fermi liquid behavior $n \sim 2$ was observed in the overdoped regime by a fit of the power law $\rho_{ab} = \rho_0 + AT^n$. It is noted that the exponent $n \sim 1.5$ in optimally doped $Ba(Fe_{1-x}Ni_x)_2As_2$ samples was reported by a different group [21]. For $Ba_{1-x}K_xFe_2As_2$ single crystals, however, it was found that ρ_{ab} actually follows a $T^{1.5}$ dependence in the optimally doped regime. And the T^2 term contributes a lot in the entire doping range $0.22 \leqslant x \leqslant 1$ [22]. In an early report

*Corresponding author: yliu@ameslab.gov

on the transport properties of $Ba_{1-x}K_xFe_2As_2$ single crystals within the low K doping regime ($0 \leqslant x \leqslant 0.4$), it was found that the power exponent n evolves from 2 for the undoped samples to 1 at optimal doping $x = 0.37$ [23]. The discrepancy may result from different temperature windows for the fits of power law and quality of single crystals. Furthermore, all superconducting $Ba_{1-x}K_xFe_2As_2$ samples from underdoped to overdoped regimes show a saturation tendency above 100 K [22].

In this study, we report the doping evolution of normal-state magnetic susceptibility, the Hall coefficient, and the Hall angle in $Ba_{1-x}K_xFe_2As_2$ ($0.13 \leqslant x \leqslant 1$) single crystals. We find that magnetic susceptibility $\chi(T)$ monotonically increases with increasing temperature for the underdoped and optimally doped samples $0.13 \leqslant x \leqslant 0.47$. A broad peak emerges as x exceeds 0.53, which suggests different magnetic interactions in the overdoped regime. Intriguingly, we observed a dramatic change of Hall coefficient R_H and Hall angle $\cot\theta_H$ as x crosses the doping $x = 0.80$, where the Lifshitz transition occurs with the change of FS topology evidenced by ARPES measurement [15] and suggested by theoretical calculations [16].

II. EXPERIMENTAL DETAILS

High-quality $Ba_{1-x}K_xFe_2As_2$ ($0.13 \leqslant x \leqslant 1$) single crystals were grown by using the self-flux method [22,24]. The crystals can be easily cleaved into thin plates along the ab plane. Magnetic susceptibility $\chi(T)$ and Hall resistivity ρ_{xy} were measured by using a physical property measurement system (PPMS, Quantum Design). For the measurements of magnetic susceptibility, the magnetic field H was applied parallel to the ab plane ($H \parallel ab$) and perpendicular to the ab plane ($H \parallel c$). Nearly ten pieces of crystals with amounts of $20 \sim 40$ mg were piled along the c axis for each measurement. In order to further clarify the intrinsic magnetic response of the samples, the magnetization as a function of applied field H was measured at a series of fixed temperatures. The temperature dependence of magnetic susceptibility curves was verified by the susceptibility data extracted from field-dependent behavior. For the high-temperature susceptibility measurements, the crystals were glued on a heat stick (PPMS VSM oven) by using cement.

The Hall resistivity ρ_{xy} was measured in magnetic field dependence at fixed temperatures. Because of the small Hall signal, misaligned contacts lead to a significant contribution to Hall voltage from the longitudinal resistivity ρ_{xx}. In order to avoid this problem, the Hall signal can be extracted from the slope of linear field dependence of Hall voltage by sweeping magnetic field. The Hall coefficient is then calculated as $R_H = \frac{V_H \times d}{I_s \times H}$, where V_H is Hall voltage, d is thickness of the thin platelike crystals, I_s is driven current, and H is applied magnetic field. The thin flakes with a thickness of 10–30 μm were obtained by peeling off single crystals using adhesive tape. Five probe contacts were made by soldering the gold wires to the single crystals. The driven current of 1 mA and 19 Hz was used in the Hall effect measurements. Two pieces of crystals were measured for each K doping to check the reproducibility of the Hall data.

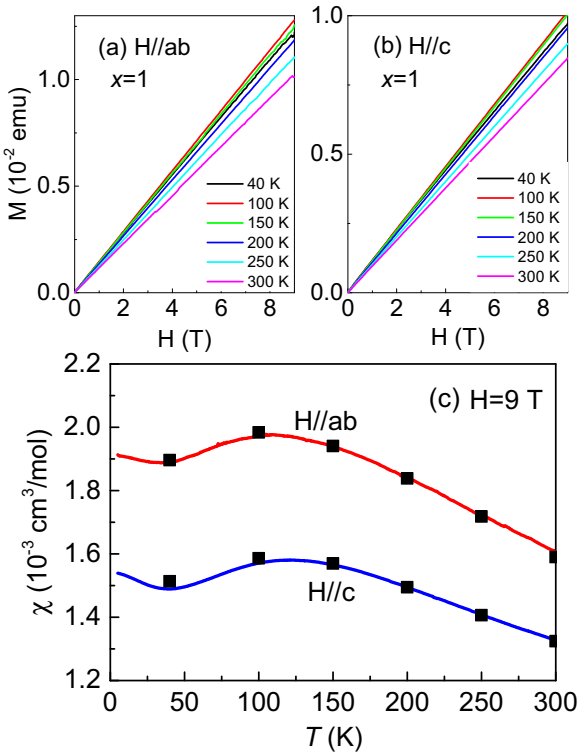

FIG. 1. (Color online) Isothermal magnetization curves of KFe_2As_2 single crystal for (a) $H \parallel ab$ and (b) $H \parallel c$, measured at 45, 100, 150, 200, 250, and 300 K. (c) Temperature dependence of magnetic susceptibility $\chi(T)$ of KFe_2As_2 single crystal is measured by an application of magnetic field of 9 T, represented by solid lines. Solid squares correspond to the susceptibility data obtained from the linear fit of isothermal magnetization curves.

III. RESULTS AND DISCUSSION

It is important to clarify the intrinsic magnetic response of iron-based superconductors because they may contain ferromagnetic inclusions [1]. Figures 1(a) and 1(b) show the isothermal magnetization curves of the KFe_2As_2 single crystal measured at 45, 100, 150, 200, 250, and 300 K in the configurations of $H \parallel ab$ and $H \parallel c$. A linear field dependence of magnetization M rules out the existence of magnetic impurity phases. Magnetic susceptibility χ is defined as $\chi = \partial M/\partial H$, i.e., the slope of the M vs H curves. The temperature dependence of the magnetic susceptibility $\chi(T)$ of the same sample was measured under a magnetic field of 9 T, as shown in Fig. 1(c). As can be seen, the susceptibility data extracted from the linear fit of isothermal magnetization curves fall on the temperature-dependent curve. A broad peak emerges at around 120 K, which is consistent with the previous results by Hardy *et al.* [25].

Figures 2(a) and 2(b) show temperature dependence of magnetic susceptibility $\chi(T)$ of $Ba_{1-x}K_xFe_2As_2$ ($0.13 \leqslant x \leqslant 1$) single crystals for $H \parallel ab$ and $H \parallel c$, respectively. Underdoped sample $x = 0.13$ displays a kink at $T_{SDW} \sim 110$ K, which matches the SDW transition temperature in the phase diagram [11,26]. Above T_{SDW}, a linear-T susceptibility $\chi(T)$ is observed. For the optimally doped samples $x = 0.34$, 0.39, and 0.47, $\chi(T)$ still maintains monotonic increase with

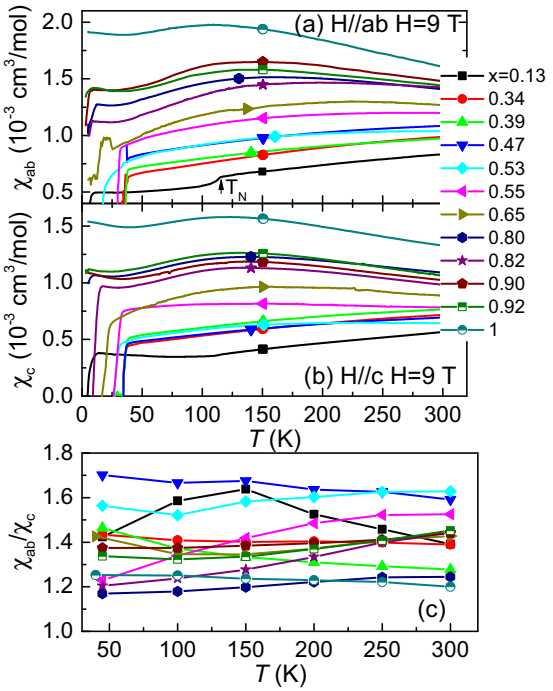

FIG. 2. (Color online) Temperature dependence of magnetic susceptibility $\chi(T)$ for $Ba_{1-x}K_xFe_2As_2$ ($0.13 \leqslant x \leqslant 1$) single crystals for (a) $H \parallel ab$ and (b) $H \parallel c$ measured under 9 T. (c) Temperature dependence of anisotropy ratio χ_{ab}/χ_c of $Ba_{1-x}K_xFe_2As_2$ single crystals.

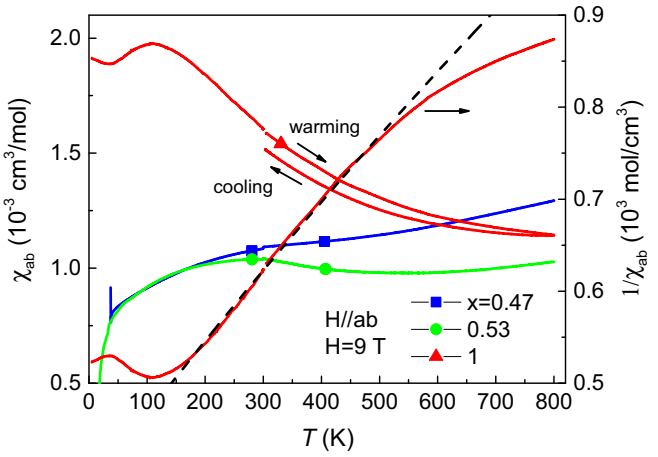

FIG. 3. (Color online) High-temperature magnetic susceptibility $\chi(T)$ up to 800 K of $Ba_{1-x}K_xFe_2As_2$ ($x = 0.47$, 0.53, and 1) single crystals. The susceptibility data of the KFe_2As_2 single crystal measured upon cooling does not follow a warming curve, which should be caused by the sample degradation at high temperature. Inverse magnetic susceptibility of the KFe_2As_2 single crystal is linked to the right axis. The dashed line corresponds to the fit of the Curie-Weiss law. The discrepancy between the susceptibility data and Curie-Weiss law above 500 K can be explained as the sample degrading above this temperature.

increasing temperature. But the susceptibility curves display a slightly down-bending behavior, not strictly following the linear relationship. With further increase of the K doping levels, $\chi(T)$ curves of overdoped samples ($0.53 \leqslant x \leqslant 0.65$) flatten out, compared to a gradual fall observed in underdoped and optimally doped samples. A big hump ranging from T_c to room temperature is observed. This big hump further evolves into a broad peak centered at 120 K for KFe_2As_2. A Curie-Weiss tail is observed at the low-temperature regime above T_c for K heavily doped samples ($0.80 \leqslant x \leqslant 1$). It is noted that the magnitude of $\chi(T)$ increases from underdoped to overdoped samples, showing a similar doping-dependent behavior to that observed in polycrystalline samples [27]. In Fig. 2(c) we show the temperature dependence of the anisotropy ratio of χ_{ab}/χ_c for all studied crystals. As can be seen, the anisotropy ratios χ_{ab}/χ_c fluctuate between 1.2 and 1.6.

In Fig. 3 we show the susceptibility data measured up to 800 K for the samples $x = 0.47$, 0.53, and 1. In order to identify the possible sample degradation at high temperatures, each measurement has been done on both warming and cooling processes. We find that magnetic susceptibility curves measured upon warming and cooling do not overlap each other but they still keep a similar temperature dependence, as shown in the case of KFe_2As_2. Here, we discuss the susceptibility data collected on the warming process. As can be seen, the susceptibility data of the sample $x = 0.47$ still follow a monotonic increase with increasing temperature. Upon warming, a down-bending behavior is observed, and $\chi(T)$ shows a weak hump centered at 300 K. The optimally doped samples $x = 0.34$ and 0.39 show a similar behavior (not shown in the figure). A clear broad hump is observed at around 300 K for the sample $x = 0.53$, while $\chi(T)$ increases again above 550 K. For the KFe_2As_2 sample, $\chi(T)$ displays a broad peak at $T = 120$ K. Above $T = 120$ K, a Curie-Weiss-like susceptibility is observed in the paramagnetic (PM) state. The inverse susceptibility of the KFe_2As_2 single crystal is shown in Fig. 3. The $\chi(T)$ data between $200 < T < 500$ K can be described by Curie-Weiss law $\chi = \frac{C}{T-\theta_p} + \chi_0$, where magnetic parameters C, θ_p, and χ_0 correspond to the Curie constant, the Curie-Weiss temperature, and the temperature-independent contribution. The large Curie-Weiss temperature θ_p of -426 K suggests dominant AFM interactions for KFe_2As_2. The effective magnetic moment $\mu_{\text{eff}} \sim 2.9\mu_B$ was calculated from the Curie constant $C = N\mu_{\text{eff}}^2/3k_B$ ($C = 1.03$). And $\chi_0 = 1.9 \times 10^{-4}$ cm^3/mol. By fixing $\chi_0 = 0$, the fit of Curie-Weiss law yields $\theta_p = -510$ K and $C = 1.3$. The effective magnetic moment μ_{eff} is estimated to be $3.2\mu_B$. Hardy *et al.* [25] had reported that $\mu_{\text{eff}} \sim 2.5\mu_B$ and $\theta_p \sim -600$ K by fitting the data between $150 < T < 300$ K.

It is still under debate as to the role of local moment in iron-based superconductors. The local Fe spin moment of parent and optimally doped $CeO_{1-x}F_xFeAs$ ($x = 0$, 0.11) and $Sr(Fe_{1-x}Co_x)_2As_2$ ($x = 0$, 0.10) has been analyzed using the Fe 3*s* core level photoemission spectra [28]. The rapid time scales of the photoemission process allowed the detection of large local spin moments fluctuating on a 10^{-15} s time scale in the PM, AFM, and superconducting phases, indicative of the occurrence of ubiquitous strong Hund magnetic correlations. An effective local spin S_{eff} was suggested as being the result of a dynamical mixing of quasidegenerate spin states of the Fe^{2+} ion by intersite electron hoppings [29]. It was found that singlet correlations among S_{eff} lead to increase of the spin

susceptibility with temperature. The theory can well explain the puzzle of large but fluctuating Fe moments [29].

In Figs. 2 and 3 we already demonstrated a crossover from the linear increase to the broad peak in $\chi(T)$ of $Ba_{1-x}K_xFe_2As_2$ single crystals. We notice that Co doping leads to a decrease of magnetic susceptibility of $Ba(Fe_{1-x}Co_x)_2As_2$ with increasing Co doping levels [30]. In the $Ba_{1-x}K_xFe_2As_2$ system, however, magnetic susceptibility is enhanced with increasing K doping levels. There are already several reports on the origin of linear-T dependence of $\chi(T)$ in iron base superconductors [31–34]. It was suggested that strong AFM fluctuations with local SDW correlation give rise to the anomalous linear-T dependence of $\chi(T)$ [31]. Soon it was argued that the linear in T term appears to be due to the nonanalytic temperature dependence of $\chi(T)$ in a two-dimensional Fermi liquid, which favors the itinerant scenario for iron pnictides [32]. Skornyakov *et al.* [33,34] further demonstrated that linear-T dependence of $\chi(T)$ in iron pnictides can be reproduced without invoking AFM fluctuations by employing the local density approximation plus the dynamical mean field method. Furthermore, contributions to the temperature dependence of the uniform susceptibility are strongly orbitally dependent. For high temperatures (>1000 K) susceptibility first saturates and then decreases with temperature [33,34]. Through ^{75}As nuclear magnetic resonance (NMR) measurements on overdoped $Ba_{1-x}K_xFe_2As_2$ ($x = 0.7$ and 1.0) single crystals, it was found that the spin-lattice relaxation $1/T_1$ dramatically increases from the sample $x = 0.7$ to the $x = 1.0$, suggesting that another type of spin fluctuation develops at the doping close to $x = 1.0$ [35]. Hirano *et al.* [36] performed ^{75}As NMR and nuclear quadrupole resonance (NQR) measurements on $Ba_{1-x}K_xFe_2As_2$ ($0.27 \leqslant x \leqslant 1$) single crystals. In the normal state, $1/T_1$ has a strong temperature dependence, which indicates the existence of large AFM spin fluctuations for all the studied crystals. Hardy *et al.* suggested that KFe_2As_2 is a strongly correlated material with highly renormalized values of both the Sommerfeld coefficient and the Pauli susceptibility [25]. The magnetic susceptibility of KFe_2As_2 can be comparable to that of the heavy fermion $CeRu_2Si_2$ which is PM state but close to AFM instability [25]. Therefore, the enhanced magnetism with increasing K content is closely related to the anomalous magnetic interactions in KFe_2As_2.

An explanation on the origin of the maximum in $\chi(T)$ of the KFe_2As_2 single crystal comes from its heavy fermion feature. The large Sommerfeld constant $\gamma_n = 94 \sim 107$ mJ/mol K^2 reported in high-quality KFe_2As_2 single crystals [25,37,38] implies a close relationship with heavy fermion compounds. Given that local moments exist in KFe_2As_2, the low-temperature maximum of $\chi(T)$ can be interpreted within the framework of two-fluid behavior suggested for the magnetic response of heavy electron materials [39,40]. The susceptibility in heavy electron materials is suggested to be the sum of three contributions: conduction electron spins χ_{cc}, local moment spins χ_{ff}, and the hybridization of conduction and localized electrons χ_{cf}. At high temperatures χ_{cc} is given by the temperature-independent Pauli susceptibility of the conduction electrons, and χ_{ff} is given by the Curie-Weiss susceptibility of the local moments. The heavy electron Kondo liquid emerges below the characteristic temperature T^* as a collective hybridization-induced instability of the spin liquid that describes the lattice of local moments coupled to background conduction electrons. Above T^*, χ_{ff} dominates. Below T^*, χ_{cf} becomes significant. T^* is determined by the effective Ruderman-Kittel-Kasuya-Yosida (RKKY) interaction between the nearest-neighbor local moments [39,40]. It is therefore suggested that the maximum in $\chi(T)$ of KFe_2As_2 indicates the growth of hybridization of conduction and localized electrons with decreasing temperature.

Let us turn to the normal-state transport properties. Figure 4 illustrates an example of how the analysis of the Hall signal was processed for the sample $x = 0.92$. The raw data can be decomposed into three terms as $V = V_{\text{offset}} + V_H H + V_{HH} H^2$, where V_{offset} corresponds to the contribution of longitudinal resistivity ρ_{xx} between the Hall contact, and V_H and V_{HH} are Hall voltages from the linear-field-dependent term and H^2 contribution, respectively. After subtracting the V_{offset} term in the raw data, Fig. 4(a) shows that the Hall voltage V_H was measured as a function of applied field by sweeping the field from −9 T to 9 T at fixed temperatures. A nearly linear field dependence of V_H is observed and the slopes dV_H/dH retain positive values. The temperature dependence of Hall coefficient R_H is shown in Fig. 4(b). The V_{offset} term presents the temperature dependence of resistivity ρ_{xx}, as shown in Fig. 4(c). The good linear field dependence of raw data confirms the very weak contribution from the H^2 term, as illustrated in Fig. 4(d).

Figure 5 shows the temperature-dependent Hall coefficient R_H of $Ba_{1-x}K_xFe_2As_2$ ($0.22 \leqslant x \leqslant 1$) single crystals. As can be seen, for the underdoped sample $x = 0.22$, R_H shows a rapid increases with decreasing temperature, and becomes a plateau at $T = 100$ K, where SDW transition occurs. For the sample $x = 0.34$, R_H gradually increases with decreasing temperature but shows a saturation tendency below $T = 150$ K. With further increasing K doping levels, R_H shows weak temperature dependence and a broad peak emerges at around 120–150 K for the samples $x = 0.47$, 0.53, 0.55, and 0.65. All the samples $x = 0.34$, 0.39, 0.47, 0.53, 0.55, and 0.65 show a convex temperature dependence below 200 K. As x exceeds 0.80, the broad peak/big hump at around 120–150 K disappears and R_H shows a rapid increases below $T = 150$ K. A peak forms below $T = 50$ K before the samples enter into superconducting state. R_H follows a concave temperature dependence within the temperature range $50 < T < 300$ K.

The doping dependence of Hall effect reflects the change of relevant electronic structure [41–43]. The knowledge about band structure and its doping evolution in $Ba_{1-x}K_xFe_2As_2$ system comes from ARPES measurements. Early ARPES data revealed that undoped ($x = 0$) and optimally doped ($x = 0.4$ and 0.45) samples have double-walled electron pocket at the M points of the BZ corner [44,45]. Zabolotnyy *et al.* [46,47] found that FS topology of the BZ corner is actually characteristic of a propeller-shaped structure, which consists of five small FS sheets: a central circular pocket surrounded by four blade-shaped pockets in $Ba_{1-x}K_xFe_2As_2$ ($x = 0$ and 0.3) single crystals. The central circular pocket around M points is electronlike, while FS sheets around the Γ point and four blade pockets are holelike. The investigation on a wide doping range of $Ba_{1-x}K_xFe_2As_2$ single crystals found that the gap size of the outer hole FS sheet around the BZ center shows an abrupt drop

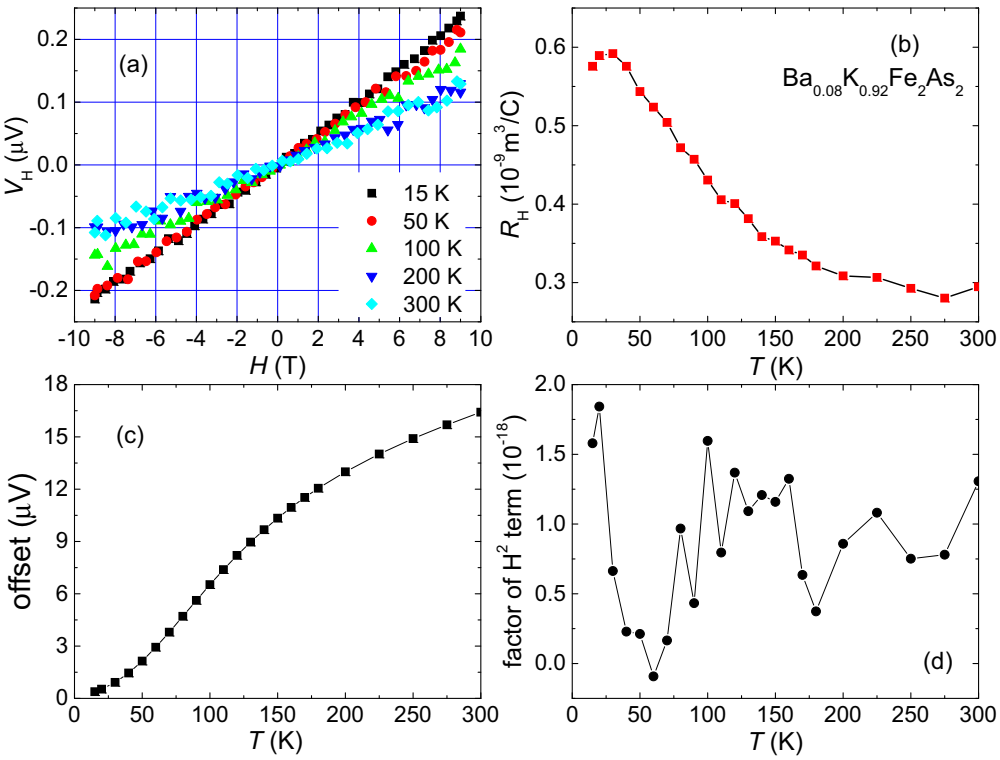

FIG. 4. (Color online) (a) Hall voltage V_H of the $Ba_{1-x}K_xFe_2As_2$ ($x = 0.92$) single crystal measured by sweeping the field from -9 T to 9 T at selected temperatures. (b) Temperature dependence of Hall coefficient R_H calculated from the linear term of the expression $V = V_{\text{offset}} + V_H H + V_{HH} H^2$. (c) The term V_{offset} in the fit of raw data corresponds to the offset caused by longitudinal resistivity ρ_{xx} between the Hall contacts. (d) The term V_{HH} evaluates the contribution from the H^2 term, which is very small and can be neglected. Solid lines are guides to the eye.

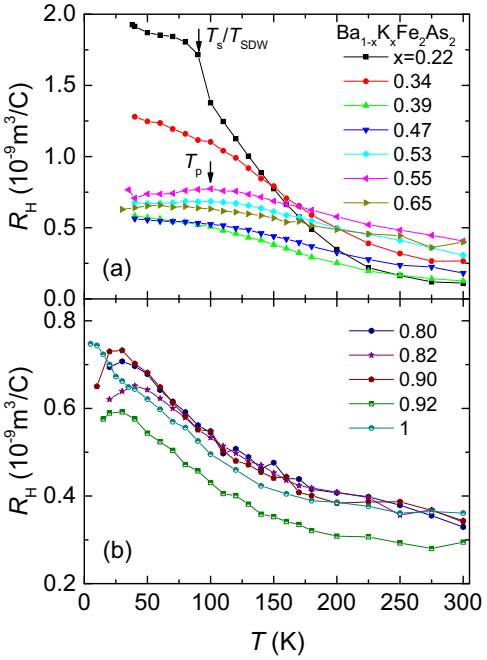

FIG. 5. (Color online) Temperature dependence of Hall coefficient R_H for $Ba_{1-x}K_xFe_2As_2$ ($0.22 \leqslant x \leqslant 0.65$) (upper panel) and ($0.80 \leqslant x \leqslant 1$) (bottom panel) single crystals. Arrows indicate the kink corresponding to the SDW transition and the broad peak observed in the samples $x = 0.53$, 0.55, and 0.65. Solid lines are guides to the eye.

with overdoping (for $x \geqslant 0.6$) while the inner and middle FS gaps roughly scale with T_c [12]. In the KFe_2As_2 single crystal, the FS around the BZ center was found to be qualitatively similar to that of the $Ba_{0.6}K_{0.4}Fe_2As_2$ single crystal, but the electron pockets centered at the M points are completely absent due to an excess of hole doping [13]. More detailed analysis of APRES data on the samples $x = 0.9$ suggested the Lifshitz transition occurred between $0.7 < x < 0.9$ [15], which is supported by the theoretical calculations [16]. Accordingly, the pairing symmetry was suggested to change from s wave in optimally doped samples to d wave in KFe_2As_2 [14]. But most possibly, the superconducting gap structure changes from the full gap state in the optimally doped samples into the nodal-line structure state for KFe_2As_2 [48,49].

It is noted that the broad peak/plateau in R_H of $Ba_{1-x}K_xFe_2As_2$ single crystals collapses in the overdoped samples ($0.80 \leqslant x \leqslant 1$), which coincides with the critical point where the electron pocket disappears and the Lifshitz transition occurs. The overall behavior of doping-dependent R_H is therefore related to the change of FS topology. Evtushinsky *et al.* [50] had calculated the temperature dependence of Hall coefficient R_H of optimally doped $Ba_{1-x}K_xFe_2As_2$ based the propeller-like FS topology observed by ARPES experiments. The agreement suggested that the temperature dependence of Hall coefficient R_H has the basis that FS evolves to a propeller-like structure at the low-temperature regime. It should be pointed out that the same maximum of R_H had been observed by Ohgushi *et al.* [51] in the Hall effect measurements

on $Ba_{1-x}K_xFe_2As_2$ ($0 \leqslant x \leqslant 0.55$) single crystals, which had been interpreted as an anomalous coherent state characterized by heavy quasiparticles in hole bands evolving below $T \sim 100$ K. The relatively weak temperature dependence observed in the optimally doped samples may suggest that incoherence-coherence crossover is less pronounced. Our results strongly suggest that the maximum of R_H observed within the doping range $0.47 \leqslant x \leqslant 0.65$ as well as the temperature-dependent behavior observed in the samples $x = 0.22$, 0.34, and 0.39 are related to the contribution from the electron pocket at the M points of the BZ. Without the contribution from the electron pocket, R_H clearly drops at around $100 < T < 150$ K. In contrast to the electron-doped $Ba(Fe_{1-x}Co_x)_2As_2$, where the hole contribution to the transport can be neglected at low temperatures in most of the phase diagram [52], electron conductivity plays a significant role in the charge transport of $Ba_{1-x}K_xFe_2As_2$ below the doping $x = 0.80$. The remarkable doping and temperature dependencies of the Hall coefficient R_H in the $Ba_{1-x}K_xFe_2As_2$ system suggest a dominant inter-band interaction between carriers having electron and hole character [53,54].

We further analyze the Hall angle $\cot\theta_H = \rho_{xx}/\rho_{xy}$ of $Ba_{1-x}K_xFe_2As_2$ ($0.22 \leqslant x \leqslant 1$) single crystals. In our analysis, both longitudinal resistivity ρ_{xx} and Hall resistivity ρ_{xy} were normalized by their room temperature values. Therefore we have

$$\cot\theta_H = \frac{\rho_{xx}}{\rho_{xy}} = \frac{\rho_{xx}}{R_H H} \propto \frac{\rho_{xx}/\rho_{xx}(300\ \mathrm{K})}{R_H/R_H(300\ \mathrm{K})}. \qquad (1)$$

The detailed analysis of doping dependence of ρ_{xx} can be found in Ref. [22]. The temperature dependence of Hall angle $\cot\theta_H$ is shown in Fig. 6. Interestingly, the Hall angle data can be clearly divided into two groups. Hall angle $\cot\theta_H$ displays a concave temperature dependence within the doping range $0.22 \leqslant x \leqslant 0.55$, whereas it changes to a convex temperature dependence within the doping range $0.65 \leqslant x \leqslant 1$. This feature again supports that the Lifshitz transition occurs at the critical doping $x = 0.65 \sim 0.80$.

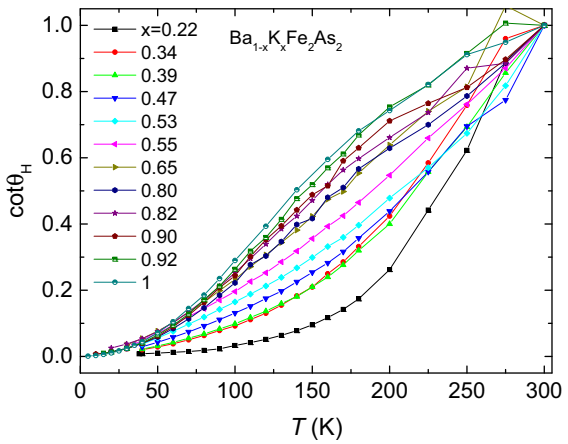

FIG. 6. (Color online) Temperature dependence of Hall angle $\cot\theta_H$ for $Ba_{1-x}K_xFe_2As_2$ ($0.22 \leqslant x \leqslant 1$) single crystals. A concave temperature dependence is observed within the doping range $0.22 \leqslant x \leqslant 0.55$, whereas it dramatically changes to a convex temperature dependence within the doping range $0.65 \leqslant x \leqslant 1$. Solid lines are guides to the eye.

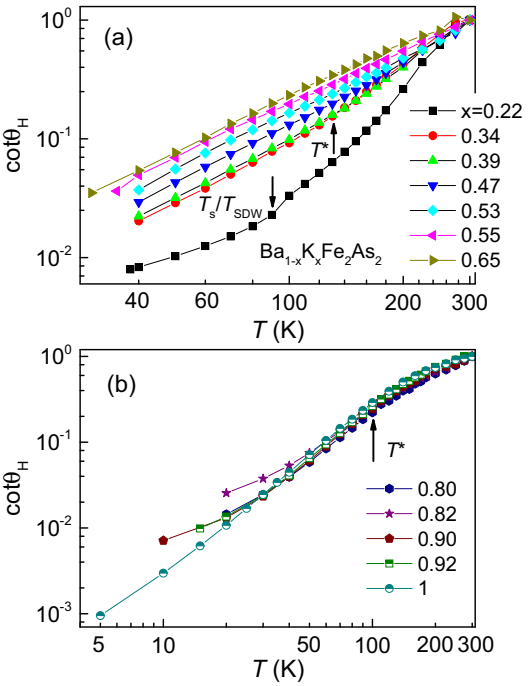

FIG. 7. (Color online) Temperature dependence of Hall angle $\cot\theta_H$ for $Ba_{1-x}K_xFe_2As_2$ ($0.22 \leqslant x \leqslant 0.65$) (upper panel) and ($0.80 \leqslant x \leqslant 1$) (bottom panel) single crystals in double logarithmic plots. The arrows indicates the kink where slopes change for the samples $x = 0.34$, 0.39, 0.47, 0.53, and 0.55 (a) and inflection point that $\cot\theta_H$ has downward curvature above it and upward curvature below it for the samples $x = 0.80$, 0.82, 0.90, 0.92, and 1 (b). Solid lines are guides to the eye.

In an early work, the power-law temperature dependent Hall angle, i.e., $\cot\theta_H = A + BT^{\alpha}$, was observed above a characteristic temperature T^* in the entire phase diagram of the $Ba_{1-x}K_xFe_2As_2$ system [55]. Figure 7 shows our Hall angle data in a double-logarithmic plot. As can be seen, there is a clear kink at around $T^* = 140$ K for the optimally doped samples $x = 0.34$, 0.39, 0.47, and 0.53. For the different dopings, T^* shifts a little bit within the temperature range $120 < T^* < 150$ K, which is quite close to the temperatures where R_H and $d\rho_{xx}/dT$ [22] display the maximum. The slopes of the double-logarithmic plots shown in Fig. 7 slightly change above and below T^*. But we can see that the temperature dependence of $\cot\theta_H$ still follows the power law below T^*. With doping approaching 0.65, the kink is smeared, and $\cot\theta_H$ follows the power law within the whole temperature range above T_c. A different behavior is observed for the samples $x = 0.80$, 0.82, 0.90, and 092. The power law (linear response) does not work well anymore. Above the characteristic temperature T^*, $\cot\theta_H$ displays the convex temperature dependence. But below T^*, the concave temperature dependence is observed. Interestingly, we found that $\cot\theta_H$ nearly follows T^2 dependence below T^* for the KFe_2As_2 single crystal. In fact, for high-quality KFe_2As_2 single crystals, ρ_{xx} follows a Fermi liquid behavior (T^2 dependence) below $T = 60$ K, while $\rho_{xx}(300\ \mathrm{K})/\rho_{xx}(4\ \mathrm{K})$

equals 780 [22]. Meanwhile, R_H only increases by a factor of 2 from 300 K to 5 K; i.e., $R_H(5\ \mathrm{K})/R_H(300\ \mathrm{K}) \sim 2$. Therefore, longitudinal resistivity ρ_{xx} actually dominates the behavior of $\cot\theta_H$, which leads to T^2 dependence of $\cot\theta_H$ at the low-temperature regime.

Finally, we discuss the correlation among magnetic susceptibility, Hall coefficient, and resistivity in $Ba_{1-x}K_xFe_2As_2$ compounds. Recently, Nakajima *et al.* reported the study of normal-state charge dynamics in $BaFe_2(As_{1-x}P_x)_2$, $Ba(Fe_{1-x}Co_x)_2As_2$, and $Ba_{1-x}K_xFe_2As_2$ through the measurements of the optical conductivity spectrum and resistivity [56]. For $BaFe_2As_2$, charge dynamics is incoherent at $T = 300$ K. The decomposition of the optical conductivity spectrum of KFe_2As_2 is nearly the same as that of $BaFe_2As_2$. The highly incoherent spectrum seems to persist over the entire doping range in the normal state of the $Ba_{1-x}K_xFe_2As_2$ system. The results strongly suggest that quasiparticle states on a substantial part of FS remain incoherent at high temperatures in the $Ba_{1-x}K_xFe_2As_2$ system [56]. Taking the two-fluid model suggested for magnetic response of heavy electron materials [39,40], the local moment spins dominate above the peak temperature T^*, whereas the hybridization of local moment spins and conduction electron spins is significant and contributes more to magnetic susceptibility below T^*. The coherent component plays a significant role below T^*, where both resistivity and susceptibility drop [56,57]. In fact, the temperature dependence of the magnetic susceptibility and the thermal expansion provide experimental evidence for the existence of a coherence-incoherence crossover in KFe_2As_2 [25]. The broad maximum at around 120 K indicates the onset of coherence. In the optimal-doping region $0.34 \leqslant x \leqslant 0.47$, SDW order is suppressed while monotonic increase of magnetic susceptibility extends to 800 K. The broad hump emerges at $x = 0.53$ and evolves into a broad peak at around 120 K in KFe_2As_2. Our magnetic susceptibility data suggest that superconductivity with high transition temperature emerges when the incoherence-coherence crossover is less pronounced in the $Ba_{1-x}K_xFe_2As_2$ system.

Resistivity of $Ba_{1-x}K_xFe_2As_2$ superconductors shows a tendency for saturation above 100 K, which gives rise to a broad peak in the plots of $d\rho_{ab}/dT$ vs T [22]. This characteristic temperature is in coincidence with the peak temperature of susceptibility curves. The Hall coefficient R_H displays weak doping and temperature dependencies above 150 K. But the low-temperature part within the doping range $0.80 \leqslant x \leqslant 1$ is quite distinct from that of the samples $0.22 \leqslant x \leqslant 0.65$. R_H tends to saturate below 150 K for the samples $0.22 \leqslant x \leqslant 0.65$, whereas it shows rapid increase for the samples $0.80 \leqslant x \leqslant 1$. It should be emphasized that the analysis of the Hall angle also supports the existence of characteristic temperature T^*, which is suggested to be related to the incoherence-coherence crossover. Assuming two types of charge careers in the $Ba_{1-x}K_xFe_2As_2$ system [56], above T^*, highly incoherent charge carriers dominate, whereas coherent ones become significant below it. Here the coherence process is related to the hybridization of conduction charge carriers and local spin moments, which gives rise to a large effective mass of conduction charge carriers. The overall behavior of magnetic susceptibility, Hall coefficient, and resistivity provides evidence of incoherence-coherence crossover at T^* in the $Ba_{1-x}K_xFe_2As_2$ system. The coherent charge dynamics in $BaFe_2(As_{1-x}P_x)_2$ and $Ba(Fe_{1-x}Co_x)_2As_2$ systems is more pronounced than the $Ba_{1-x}K_xFe_2As_2$ system in the normal state [56]. It could be the reason why the coherence-incoherence crossover is not observed in resistivity and magnetic susceptibility of $BaFe_2(As_{1-x}P_x)_2$ and $Ba(Fe_{1-x}Co_x)_2As_2$ systems.

IV. CONCLUSIONS

In summary, we have performed magnetic susceptibility $\chi(T)$ and Hall coefficient R_H measurements on a series of $Ba_{1-x}K_xFe_2As_2$ single crystals. A crossover from the SDW ordered state to KFe_2As_2-type magnetic interactions occurs with increasing K content. It is found that $\chi(T)$ monotonically increases with increasing temperature for the underdoped and optimally doped samples $0.13 \leqslant x \leqslant 0.47$. For the overdoped samples $0.53 \leqslant x \leqslant 1$, a big hump was observed at around 150 K, and it eventually evolves into a broad peak in KFe_2As_2 at 120 K. The magnitude of magnetic susceptibility keeps increasing with increasing K content. The Hall coefficient R_H and Hall angle $\cot\theta_H$ display a dramatic change as x exceeds 0.80, which coincides with the critical doping point where the electron pocket disappears with excess hole doping. Our results strongly support that the change of doping dependence of Hall coefficient R_H and Hall angle $\cot\theta_H$ is related to the change of FS topology, i.e., the Lifshitz transition. The characteristic temperature T^* is identified in magnetic susceptibility, Hall coefficient, and resistivity data, which strongly suggests the incoherence-coherence crossover occurred in the $Ba_{1-x}K_xFe_2As_2$ system.

ACKNOWLEDGMENTS

This work was supported by the US Department of Energy (DOE), Office of Science, Basic Energy Sciences, Materials Science and Engineering Division. The research was performed at the Ames Laboratory, which is operated for the US DOE by Iowa State University under Contract No. DE-AC02-07CH11358.

[1] D. C. Johnston, Adv. Phys. **59**, 803 (2010).
[2] G. R. Stewart, Rev. Mod. Phys. **83**, 1589 (2011).
[3] M. D. Lumsden and A. D. Christianson, J. Phys.: Condens. Matter **22**, 203203 (2010).
[4] P. Dai, J. Hu, and E. Dagotto, Nat. Phys. **8**, 709 (2012).
[5] P. J. Hirschfeld, M. M. Korshunov, and I. I. Mazin, Rep. Prog. Phys. **74**, 124508 (2011).
[6] A. Chubukov, Annu. Rev. Condens. Matter Phys. **3**, 57 (2012).
[7] J. Dong, H. J. Zhang, G. Xu, Z. Li, G. Li, W. Z. Hu, D. Wu, G. F. Chen, X. Dai, J. L. Luo, Z. Fang, and N. L. Wang, Europhys. Lett. **83**, 27006 (2008).

[8] M. Rotter, M. Tegel, D. Johrendt, I. Schellenberg, W. Hermes, and R. Pöttgen, Phys. Rev. B **78**, 020503(R) (2008).

[9] K. Haule, J. H. Shim, and G. Kotliar, Phys. Rev. Lett. **100**, 226402 (2008).

[10] I. I. Mazin, D. J. Singh, M. D. Johannes, and M. H. Du, Phys. Rev. Lett. **101**, 057003 (2008).

[11] M. Rotter, M. Pangerl, M. Tegel, and D. Johrendt, Angew. Chem. Int. Ed. **47**, 7949 (2008).

[12] W. Malaeb, T. Shimojima, Y. Ishida, K. Okazaki, Y. Ota, K. Ohgushi, K. Kihou, T. Saito, C. H. Lee, S. Ishida, M. Nakajima, S. Uchida, H. Fukazawa, Y. Kohori, A. Iyo, H. Eisaki, C.-T. Chen, S. Watanabe, H. Ikeda, and S. Shin, Phys. Rev. B **86**, 165117 (2012).

[13] T. Sato, K. Nakayama, Y. Sekiba, P. Richard, Y.-M. Xu, S. Souma, T. Takahashi, G. F. Chen, J. L. Luo, N. L. Wang, and H. Ding, Phys. Rev. Lett. **103**, 047002 (2009).

[14] J.-Ph. Reid, M. A. Tanatar, A. Juneau-Fecteau, R. T. Gordon, S. R. de Cotret, N. Doiron-Leyraud, T. Saito, H. Fukazawa, Y. Kohori, K. Kihou, C. H. Lee, A. Iyo, H. Eisaki, R. Prozorov, and Louis Taillefer, Phys. Rev. Lett. **109**, 087001 (2012).

[15] N. Xu, P. Richard, X. Shi, A. van Roekeghem, T. Qian, E. Razzoli, E. Rienks, G.-F. Chen, E. Ieki, K. Nakayama, T. Sato, T. Takahashi, M. Shi, and H. Ding, Phys. Rev. B **88**, 220508(R) (2013).

[16] S. N. Khan and D. D. Johnson, Phys. Rev. Lett. **112**, 156401 (2014).

[17] H. Hodovanets, Y. Liu, A. Jesche, S. Ran, E. D. Mun, T. A. Lograsso, S. L. Bud'ko, and P. C. Canfield, Phys. Rev. B **89**, 224517 (2014).

[18] S. Kasahara, T. Shibauchi, K. Hashimoto, K. Ikada, S. Tonegawa, R. Okazaki, H. Shishido, H. Ikeda, H. Takeya, K. Hirata, T. Terashima, and Y. Matsuda, Phys. Rev. B **81**, 184519 (2010).

[19] G. N. Tam, B. D. Faeth, J. S. Kim, and G. R. Stewart, Phys. Rev. B **88**, 134503 (2013).

[20] R. Zhou, Z. Li, J. Yang, D. L. Sun, C. T. Lin, and G.-q. Zheng, Nat. Commun. **4**, 2265 (2013).

[21] H. Luo, R. Zhang, M. Laver, Z. Yamani, M. Wang, X. Lu, M. Wang, Y. Chen, S. Li, S. Chang, J. W. Lynn, and P. Dai, Phys. Rev. Lett. **108**, 247002 (2012).

[22] Y. Liu, M. A. Tanatar, W. E. Straszheim, B. Jensen, K. W. Dennis, R. W. McCallum, V. G. Kogan, R. Prozorov, and T. A. Lograsso, Phys. Rev. B **89**, 134504 (2014).

[23] B. Shen, H. Yang, Z.-S. Wang, F. Han, B. Zeng, L. Shan, C. Ren, and H.-H. Wen, Phys. Rev. B **84**, 184512 (2011).

[24] Y. Liu, M. A. Tanatar, V. G. Kogan, H. Kim, T. A. Lograsso, and R. Prozorov, Phys. Rev. B **87**, 134513 (2013).

[25] F. Hardy, A. E. Böhmer, D. Aoki, P. Burger, T. Wolf, P. Schweiss, R. Heid, P. Adelmann, Y. X. Yao, G. Kotliar, J. Schmalian, and C. Meingast, Phys. Rev. Lett. **111**, 027002 (2013).

[26] S. Avci, O. Chmaissem, D. Y. Chung, S. Rosenkranz, E. A. Goremychkin, J. P. Castellan, I. S. Todorov, J. A. Schlueter, H. Claus, A. Daoud-Aladine, D. D. Khalyavin, M. G. Kanatzidis, and R. Osborn, Phys. Rev. B **85**, 184507 (2012).

[27] J. G. Storey, J. W. Loram, J. R. Cooper, Z. Bukowski, and J. Karpinski, Phys. Rev. B **88**, 144502 (2013).

[28] P. Vilmercati, A. Fedorov, F. Bondino, F. Offi, G. Panaccione, P. Lacovig, L. Simonelli, M. A. McGuire, A. S. M. Sefat, D. Mandrus, B. C. Sales, T. Egami, W. Ku, and N. Mannella, Phys. Rev. B **85**, 220503(R) (2012).

[29] J. Chaloupka and G. Khaliullin, Phys. Rev. Lett. **110**, 207205 (2013).

[30] X. F. Wang, T. Wu, G. Wu, R. H. Liu, H. Chen, Y. L. Xie, and X. H. Chen, New J. Phys. **11**, 045003 (2009).

[31] G. M. Zhang, Y. H. Su, Z. Y. Lu, Z. Y. Weng, D. H. Lee, and T. Xiang, Europhys. Lett. **86**, 37006 (2009).

[32] M. M. Korshunov, I. Eremin, D. V. Efremov, D. L. Maslov, and A. V. Chubukov, Phys. Rev. Lett. **102**, 236403 (2009).

[33] S. L. Skornyakov, A. A. Katanin, and V. I. Anisimov, Phys. Rev. Lett. **106**, 047007 (2011).

[34] S. L. Skornyakov, V. I. Anisimov, and D. Vollhardt, Phys. Rev. B **86**, 125124 (2012).

[35] S. W. Zhang, L. Ma, Y. D. Hou, J. Zhang, T.-L. Xia, G. F. Chen, J. P. Hu, G. M. Luke, and W. Yu, Phys. Rev. B **81**, 012503 (2010).

[36] M. Hirano, Y. Yamada, T. Saito, R. Nagashima, T. Konishi, T. Toriyama, Y. Ohta, H. Fukazawa, Y. Kohori, Y. Furukawa, K. Kihou, C.-H. Lee, A. Iyo, and H. Eisaki, J. Phys. Soc. Jpn. **81**, 054704 (2012).

[37] M. Abdel-Hafiez, S. Aswartham, S. Wurmehl, V. Grinenko, C. Hess, S.-L. Drechsler, S. Johnston, A. U. B. Wolter, B. Büchner, H. Rosner, and L. Boeri, Phys. Rev. B **85**, 134533 (2012).

[38] S. L. Bud'ko, Y. Liu, T. A. Lograsso, and P. C. Canfield, Phys. Rev. B **86**, 224514 (2012).

[39] Y.-F. Yang and D. Pines, Proc. Natl. Acad. Sci. USA **109**, E3060 (2012).

[40] K. R. Shirer, A. C. Shockley, A. P. Dioguardi, J. Crocker, C. H. Lin, N. apRoberts-Warren, D. M. Nisson, P. Klavins, J. C. Cooley, Y.-F. Yang, and N. J. Curro, Proc. Natl. Acad. Sci. USA **109**, E3067 (2012).

[41] C. Kittel, *Introduction to Solid State Physics*, 8th ed. (John Wiley & Sons, Hoboken, NJ, 2004).

[42] Neil W. Ashcroft and N. David Mermin, *Solid State Physics* (Brooks/Cole, Belmont, CA, 1976).

[43] Colin M. Hurd, *The Hall Effect in Metals and Alloys* (Plenum Press, New York, 1972).

[44] H. Ding, P. Richard, K. Nakayama, K. Sugawara, T. Arakane, Y. Sekiba, A. Takayama, S. Souma, T. Sato, T. Takahashi, Z. Wang, X. Dai, Z. Fang, G. F. Chen, J. L. Luo, and N. L. Wang, Europhys. Lett. **83**, 47001 (2008).

[45] C. Liu, G. D. Samolyuk, Y. Lee, N. Ni, T. Kondo, A. F. Santander-Syro, S. L. Bud'ko, J. L. McChesney, E. Rotenberg, T. Valla, A. V. Fedorov, P. C. Canfield, B. N. Harmon, and A. Kaminski, Phys. Rev. Lett. **101**, 177005 (2008).

[46] V. B. Zabolotnyy, D. S. Inosov, D. V. Evtushinsky, A. Koitzsch, A. A. Kordyuk, G. L. Sun, J. T. Park, D. Haug, V. Hinkov, A. V. Boris, C. T. Lin, M. Knupfer, A. N. Yaresko, B. Büchner, A. Varykhalov, R. Follath, and S. V. Borisenko, Nature (London) **457**, 569 (2009).

[47] D. V. Evtushinsky, D. S. Inosov, V. B. Zabolotnyy, A. Koitzsch, M. Knupfer, B. Büchner, M. S. Viazovska, G. L. Sun, V. Hinkov, A. V. Boris, C. T. Lin, B. Keimer, A. Varykhalov, A. A. Kordyuk, and S. V. Borisenko, Phys. Rev. B **79**, 054517 (2009).

[48] K. Okazaki, Y. Ota, Y. Kotani, W. Malaeb, Y. Ishida, T. Shimojima, T. Kiss, S. Watanabe, C.-T. Chen, K. Kihou, C. H. Lee, A. Iyo, H. Eisaki, T. Saito, H. Fukazawa, Y. Kohori, K. Hashimoto, T. Shibauchi, Y. Matsuda, H. Ikeda, H. Miyahara, R. Arita, A. Chainani, and S. Shin, Science **337**, 1314 (2012).

[49] M. Hirano, Y. Yamada, T. Saito, Y. Murano, R. Nagashima, H. Fukazawa, Y. Kohori, Y. Furukawa, K. Kihou, C. H. Lee, A. Iyo, and H. Eisaki, J. Phys.: Conf. Ser. **400**, 022026 (2012).

[50] D. V. Evtushinsky, A. A. Kordyuk, V. B. Zabolotnyy, D. S. Inosov, T. K. Kim, B. Büchner, H. Luo, Z. Wang, H.-H. Wen, G. Sun, C. Lin, and S. V. Borisenko, J. Phys. Soc. Jpn. **80**, 023710 (2011).

[51] K. Ohgushi and Y. Kiuchi, Phys. Rev. B **85**, 064522 (2012).

[52] F. Rullier-Albenque, D. Colson, A. Forget, and H. Alloul, Phys. Rev. Lett. **103**, 057001 (2009).

[53] L. Fanfarillo, E. Cappelluti, C. Castellani, and L. Benfatto, Phys. Rev. Lett. **109**, 096402 (2012).

[54] A. F. Kemper, M. M. Korshunov, T. P. Devereaux, J. N. Fry, H-P. Cheng, and P. J. Hirschfeld, Phys. Rev. B **83**, 184516 (2011).

[55] Y. J. Yan, A. F. Wang, X. G. Luo, Z. Sun, J. J. Ying, G. J. Ye, P. Chen, J. Q. Ma, and X. H. Chen, arXiv:1301.1734.

[56] M. Nakajima, S. Ishida, T. Tanaka, K. Kihou, Y. Tomioka, T. Saito, C. H. Lee, H. Fukazawa, Y. Kohori, T. Kakeshita, A. Iyo, T. Ito, H. Eisaki, and S. Uchida, Sci. Rep. **4**, 5873 (2014).

[57] K. Haule and G. Kotliar, New J. Phys. **11**, 025021 (2009).